# EQUILIBRIUM AND STABILITY

# OF RECTANGULAR LIQUID-FILLED VESSELS

A Senior Scholars Thesis

by

RUSSELL TRAHAN III

Submitted to the Office of Undergraduate Research
Texas A&M University
in partial fulfillment of the requirements for the designation as

UNDERGRADUATE RESEARCH SCHOLAR

April 2010

Major: Aerospace Engineering

# EQUILIBRIUM AND STABILITY

# OF RECTANGULAR LIQUID-FILLED VESSELS

A Senior Scholars Thesis

by

RUSSELL TRAHAN III

Submitted to the Office of Undergraduate Research
Texas A&M University
in partial fulfillment of the requirements for the designation as

UNDERGRADUATE RESEARCH SCHOLAR

Approved by:

| | |
|---|---|
| Research Advisor: | Tamás Kalmár-Nagy |
| Associate Dean for Undergraduate Research: | Robert C. Webb |

April 2010

Major: Aerospace Engineering

# ABSTRACT

Equilibrium and Stability of Rectangular Liquid-Filled Vessels.
(April 2010)

Russell Trahan III
Department of Aerospace Engineering
Texas A&M University

Research Advisor: Tamás Kalmár-Nagy
Department of Aerospace Engineering

Here we focus on the stability characteristics of a rectangular liquid-filled vessel. The position vector of the center of gravity of the liquid volume is derived and used to express the equilibrium angles of the vessel. Analysis of the potential function determines the stability of these equilibria, and bifurcation diagrams are constructed to demonstrate the co-existence of several equilibrium configurations of the vessel. To validate the results, a vessel of rectangular cross-section was built. The results of the experiments agree well with the theoretical predictions.

# ACKNOWLEDGEMENTS

Valuable discussions on the topic with Gabor Stépán and financial support by the US Air Force Office of Scientific Research (Grant No. AFOSR-06-0787) are gratefully acknowledged.

# TABLE OF CONTENTS

Page

# LIST OF FIGURES

FIGURE Page

# CHAPTER I

# INTRODUCTION

Determining equilibrium positions of structures and characterizing their stability is a common engineering task. Fluid-structure interactions are one of the many stability concerns in dynamic systems. For example, some marine structures such as floating oil rigs and dry-docks use water as ballast to stabilize the structure. Vehicles such as aircraft, boats, and machinery operate under conditions where the fuel tank or liquid payload may adversely affect the stability of the vehicle due to sloshing[13]. Determining the behavior of the liquid in a tank is an important consideration in the design and analysis of these devices. These examples provide the motivation for our stability analysis of a rectangular liquid-filled vessel.

This paper discusses the static stability of a vessel with a rectangular cross section that can pivot about a fixed point and contains liquid[4]. An equally important purpose for this paper is to present an example through which the concepts of bifurcations, potential functions, and stability of non-linear physical systems becomes more available to students. The experimental setup described here is easy to build and may serve as an effective classroom demonstration. A similar system -a hanging block- is studied by Stépán and Bianchi (1994). They characterize the stability of a mass hanging from two

---

This thesis follows the style of American Journal of Physics.

ropes by using a potential function depending on various geometric parameters of the system.

Research into the stability of floating bodies has a long history, starting with Archimedes' *On Floating Bodies*. The ship problem asks to relate the buoyancy force to ship stability. Locating equilibrium positions of floating objects and ascertaining the stability of these equilibria is not a trivial exercise. Duffy (1993) consider the equilibrium positions of partially submerged rods supported at one end and show the existence of simple bifurcations and the jump phenomenon (hysteresis) in the problem. Erdös et al. (1992) investigate the equilibrium configurations for floating solid prisms of square and equilateral triangular cross-section. Delbourgo (1987) provides a solution to the metacentric problem for a floating plank. Our system can be thought of as an inverted ship problem (for the ship problem, the body is submerged in the liquid). While Delbourgo's problem is analogous to ours and his results are similar, we believe that our exposition is more detailed and lucid, thereby making this type of problems more known to the nonlinear dynamics community.

We start by defining the geometry of the vessel and the liquid contained within in Section 0. The physical parameters that are varied are the amount of liquid, the pivot-height to vessel-width ratio, and the angle of rotation about the pivot. The algebraic equations describing the location of the center of gravity of the liquid are derived. From these equations, the equilibrium positions of the vessel are expressed in Section 0. The stability of the equilibrium positions is determined with a potential function. The results

from the equilibrium calculations and stability analysis are used to construct bifurcation diagrams for various physical parameters of the vessel in Section 0. These diagrams are then compared to experimental data in Section 0.

# CHAPTER II

# PROBLEM DEFINITION AND ASSUMPTIONS

The object of our study (hereupon called vessel) is illustrated in Figure 1. We are concerned with static equilibrium states of the vessel-liquid system and their stability. All dynamic effects are excluded, including angular acceleration of the system and sloshing of the liquid. We assume that the walls of the vessel have negligible thickness. Furthermore, the vessel is assumed to be tall enough to avoid spillage.

The vessel has a rectangular cross section -characterized by the width $W$- and contains a liquid with cross-sectional area of $H \cdot W$. The distance of the pivot from the base is $P$. Figure 2 depicts a situation when the vessel is rotated about the pivot by angle $\theta$. Hereon, we illustrate the liquid rotated and the vessel stationary for simplicity.

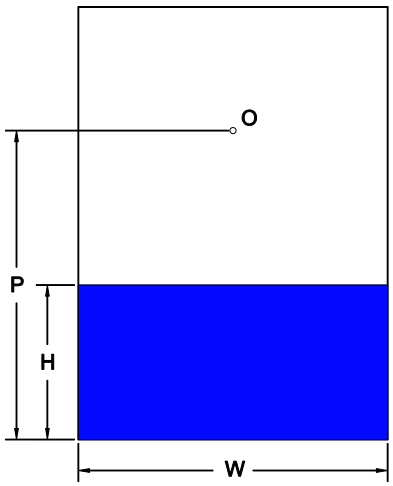

Figure 1: Vessel geometry

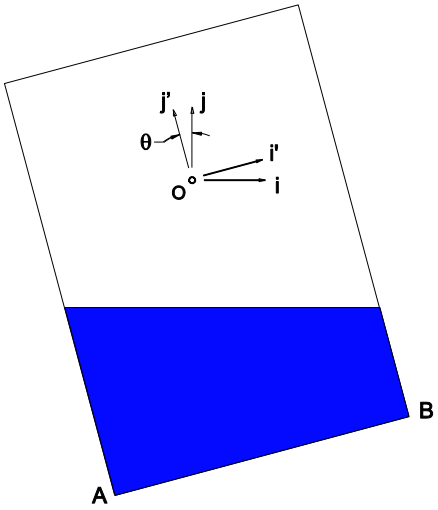

Figure 2: Liquid cross-section geometry

All parameters are non-dimensionalized by scaling with the pivot height *P*, i.e.

$$h = \frac{H}{P}$$

$$w = \frac{W}{P}$$

Without loss of generality (due to the symmetry of the vessel), we will assume non-negative $\theta$ in the calculations[8]. Using the coordinate system defined in Figure 2, the position vectors for the bottom corners of the vessel, A and B, relative to O can be expressed in terms of $\theta \geq 0$ as

$$\vec{r}_A = \left( \sin\theta - \frac{w}{2}\cos\theta \right)\hat{i} - \left( \cos\theta + \frac{w}{2} \right)\hat{j}$$

$$\vec{r}_B = \left( \sin\theta + \frac{w}{2}\cos\theta \right)\hat{i} - \left( \cos\theta - \frac{w}{2} \right)\hat{j}$$

These expressions will later be used to derive the location of the center of gravity (CG) of the liquid cross-section.

**Geometric cases**

The shape of the liquid's cross-section is dependent on the pivot angle $\theta$ and amount of liquid in the vessel. The cross-section could either be trapezoidal (Figure 3a) or triangular (Figure 3b), referred to as Case 1 and Case 2, respectively.

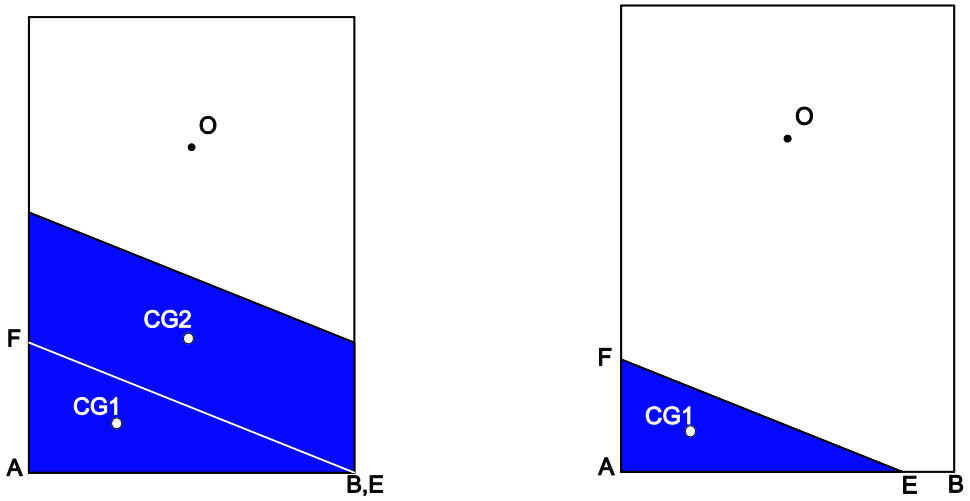


a) Case 1 b) Case 2

Figure 3: Vessel cases

The triangular section of liquid is defined by the points A, E and F. The relative positions of points E and F with respect to A are expressed by

$$\vec{r}_{E/A} = \max\left(w, \sqrt{2\frac{hw}{\tan\theta}}\right)\hat{i}' \quad (1)$$

$$\vec{r}_{F/A} = \sqrt{2hw\tan\theta}\,\hat{j}' \quad (2)$$

Equation (1) expresses that $r_{E/A} = |\vec{r}_{E/A}|$ is physically limited to the vessel-width, i.e. $r_{E/A} \le w$. This constraint results in the two cases mentioned above, i.e. trapezoidal (Case 1) or triangular (Case 2) cross-section, characterized by the inequalities

$$\text{Case 1: } \tan\theta < \frac{2h}{w}, \tag{3}$$

$$\text{Case 2: } \tan\theta \ge \frac{2h}{w}. \tag{4}$$

**Center of gravity**

The equilibria of the vessel are determined by first finding the center of gravity (CG) of the liquid. CG1 (cf. Figure 3) is located at the centroid of the triangle, and CG2 is located at the centroid of the parallelogram.

$$\begin{aligned}\vec{r}_{CG1} = &\left[\left(\frac{\sqrt{2}}{3}\sqrt{\frac{hw}{\tan\theta}} - \frac{w}{2}\right)\cos\theta + \left(1 - \frac{\sqrt{2hw\tan\theta}}{3}\right)\sin\theta\right]\hat{i} \\ &+\left[\left(\frac{\sqrt{2hw\tan\theta}}{3} - 1\right)\cos\theta + \left(\frac{\sqrt{2}}{3}\sqrt{\frac{hw}{\tan\theta}} - \frac{w}{2}\right)\sin\theta\right]\hat{j},\end{aligned} \tag{5}$$

$$\vec{r}_{CG2} = \left(1 - \frac{w\tan\theta}{4} - \frac{h}{2}\right)\sin\theta\hat{i} + \left(\left(\frac{h}{2} - 1\right)\cos\theta + \frac{w}{4}\sin\theta\right)\hat{j}. \tag{6}$$

The CG for the whole liquid cross-section is calculated using a weighted average of the coordinates of the two CGs and the corresponding areas $A_1$ and $A_2$, i.e.

$$\vec{r}_{CG} = \frac{\vec{r}_{CG1}A_1 + \vec{r}_{CG2}A_2}{A_1 + A_2}, \tag{7}$$

where the areas are

$$A_1 = \begin{cases} w^2 \tan\theta & \text{Case 1} \\ hw & \text{Case 2} \end{cases}, \qquad A_2 = \begin{cases} hw - w^2 \tan\theta & \text{Case 1} \\ 0 & \text{Case 2.} \end{cases} \tag{8}$$

The center of gravity of the liquid cross-section is thus given by

$$\vec{r}_{CG} = \begin{cases} \left(1 - \dfrac{w^2 \tan^2\theta}{24h} - \dfrac{w^2}{12h} - \dfrac{h}{2}\right)\sin\theta\hat{\mathrm{i}} + \left(\left(\dfrac{\mathrm{h}}{2}\text{-}1\right)\cos\theta + \dfrac{\mathrm{w}^2 \tan\theta \sin\theta}{24\mathrm{h}}\right)\hat{\mathrm{j}}, & \text{Case 1} \\ \left[\left(\dfrac{\sqrt{2}}{3}\sqrt{\dfrac{hw}{\tan\theta}} - \dfrac{w}{2}\right)\cos\theta + \left(1 - \dfrac{\sqrt{2hw\tan\theta}}{3}\right)\sin\theta\right]\hat{i} + & \text{Case 2} \\ \quad \left[\left(\dfrac{\sqrt{2hw\tan\theta}}{3} - 1\right)\cos\theta + \left(\dfrac{\sqrt{2}}{3}\sqrt{\dfrac{hw}{\tan\theta}} - \dfrac{w}{2}\right)\sin\theta\right]\hat{j}. & \end{cases} \tag{9}$$

# CHAPTER III

# POTENTIAL FUNCTION, EQUILIBRIA, AND STABILITY

The equilibrium angles of the vessel and their stability are determined by analyzing the non-dimensional potential function[6] defined by the $\hat{j}$ component of the CG location:

$$U \equiv \vec{r}_{CG} \cdot \hat{j} = \begin{cases} \left(\frac{h}{2} - 1\right)\cos\theta - \frac{w^2 \tan\theta \sin\theta}{24h}, & \text{Case 1} \\ \left(\frac{\sqrt{2hw\tan\theta}}{3} - 1\right)\cos\theta + \left(\frac{\sqrt{2}}{3}\sqrt{\frac{hw}{\tan\theta}} - \frac{w}{2}\right)\sin\theta. & \text{Case 2} \end{cases} \tag{10}$$

Physically, the vessel is in equilibrium when the CG of the cross-section of the liquid is on the vertical axis. This is expressed as $\vec{r}_{CG} \cdot \hat{i} = 0$. It is also true that $\vec{r}_{CG} \cdot \hat{i} = 0$ corresponds to local extrema of the potential function, i.e.

$$\frac{dU}{d\theta} = 0 = \begin{cases} \left(1 - \frac{w^2 \tan^2\theta}{24h} - \frac{w^2}{12h} - \frac{h}{2}\right)\sin\theta, & \text{Case 1} \\ \frac{\sqrt{2hw}}{3} - \frac{w}{2}\tan^{\frac{1}{2}}\theta + \tan^{\frac{3}{2}}\theta - \frac{\sqrt{2hw}}{3}\tan^2\theta. & \text{Case 2} \end{cases} \tag{11}$$

We will later use the second derivative of the potential function to classify the stability of particular equilibria.

**Equilibria conditions**

Plotted in Figure 4 are the non-zero equilibrium positions given by equation (11) in *h*-*w*-$\theta$ space. The left and right shaded regions depict Case 2 and Case 1 equilibria respectively.

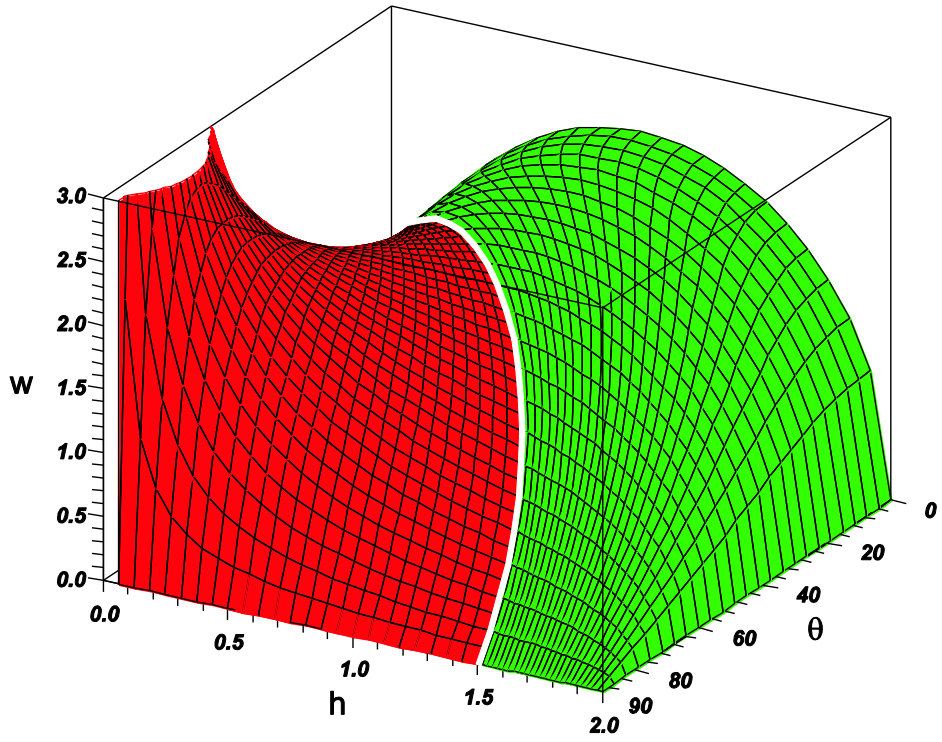


Figure 4: *h*-*w*-$\theta$ plot of $\theta \neq 0$ equilibria

As can be observed, for a given value of *h* and *w*, multiple $\theta$ solutions can exist. We now define the domains in which different numbers of equilibria exist[9].

Case 1 equilibria are determined by (cf. equation (11))

$$\left(1-\frac{w^2\tan^2\theta}{24h}-\frac{w^2}{12h}-\frac{h}{2}\right)\sin\theta=0, \qquad 0\le\tan\theta<\frac{2h}{w}. \tag{12}$$

Clearly, $\theta$=0 is always a solution. Other solutions satisfy

$$\tan^2\theta = \left(2h - h^2\right)\frac{12}{w^2} - 2, \qquad 0 < \tan\theta < \frac{2h}{w}. \tag{13}$$

Expression (13) is equivalent to the two inequalities

$$\left(h-1\right)^2 + \frac{w^2}{6} \le 1, \tag{14}$$

$$\left(h - \frac{3}{4}\right)^2 + \frac{w^2}{8} \ge \frac{9}{16}, \tag{15}$$

which determine that a positive $\theta$ solution exists between the two half-ellipses shown in Figure 5. For later reference, we refer to equation $\left(h-1\right)^2 + \frac{w^2}{6} = 1$ as curve I.

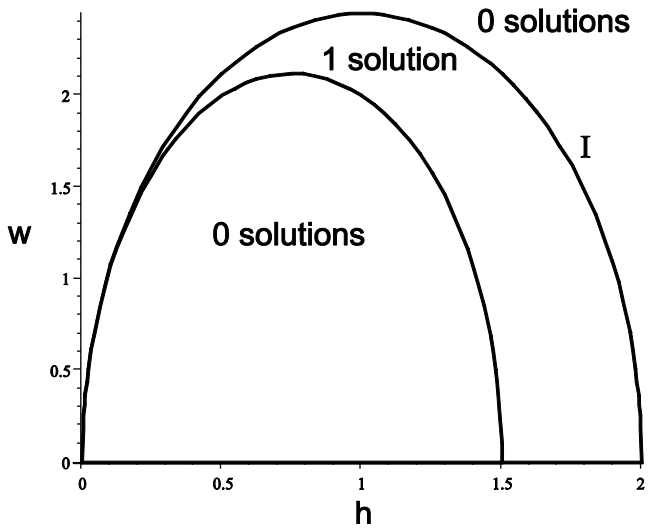


Figure 5: Number of solutions of expression (13)

Case 2 equilibria are given by

$$\frac{\sqrt{2hw}}{3}-\frac{w}{2}\tan^{\frac{1}{2}}\theta+\tan^{\frac{3}{2}}\theta-\frac{\sqrt{2hw}}{3}\tan^{2}\theta=0, \tag{16}$$

subject to the constraint

$$\tan\theta\geq\frac{2h}{w}. \tag{17}$$

It can be shown that equation (16) has three non-negative roots. The regions in h-w space with one or three real roots are separated by a curve on which equation (16) has a double root. For equation (16) to have a double root it is necessary that its derivative vanishes, i.e.

$$-3w+18\tan\theta-8\sqrt{2}\sqrt{hw}\tan^{3/2}\theta=0. \tag{18}$$

Equations (16) and (18) are now combined and solved for *h* and *w* to give the boundary in parametric form in terms of $\theta$ as

$$h(\theta)=\frac{9\tan^{2}\theta}{\left(\tan^{2}\theta+3\right)\left(3\tan^{2}\theta+1\right)}, \tag{19}$$

$$w(\theta)=\frac{2\tan\theta\left(\tan^{2}\theta+3\right)}{3\tan^{2}\theta+1}. \tag{20}$$

The parametric curve, referred to as curve II, $\{h(\theta),w(\theta)\}$ is plotted in Figure 6. The region left of the curve is where equation (16) has three real roots.[2]

Substituting the constraint (17) into equation (16) gives

[2] This statement can be proved by considering the *h*=0, *w*=2 case. Equation (16) reduces to $\tan^{3}\theta-\tan\theta=0$, which clearly has three real roots. By a continuity argument, equation (16) has three real roots in the region left of the double root curve.

$$-12h^{3/2}\sqrt{w}+8h^{5/2}\sqrt{w}+\sqrt{h}w^{5/2}\geq 0, \tag{21}$$

which can also be expressed as

$$\left(h-\frac{3}{4}\right)^2+\frac{w^2}{8}\leq\frac{9}{16}. \tag{22}$$

Outside of this elliptical region (bounded by curve I), one of the possible real roots does not satisfy constraint (17). Figure 7 shows the number of valid Case 2 solutions in the *h*-*w* plane.

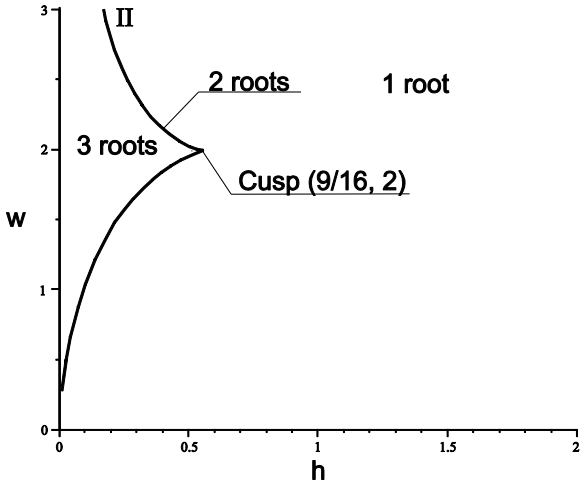


Figure 6: Number of real roots in equation (16)

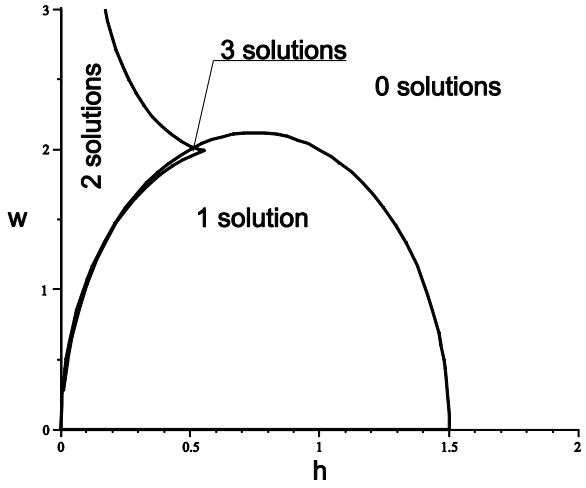


Figure 7: Number of solutions in equation (16) with contraint (17)

We are now in a position to present information about all equilibria of the vessel. Recall that in the calculations $\theta$ was assumed to be non-negative. Without this restriction each Case 1 and Case 2 solution corresponds to two equilibrium configurations of the vessel, resulting in an odd number of equilibria for the system ($\theta$ =0, Case 1, and Case 2 equilibria). Figure 8 shows the various regions and indicates the total number of equilibria. The gray region is where Case 2 equilibria are present.

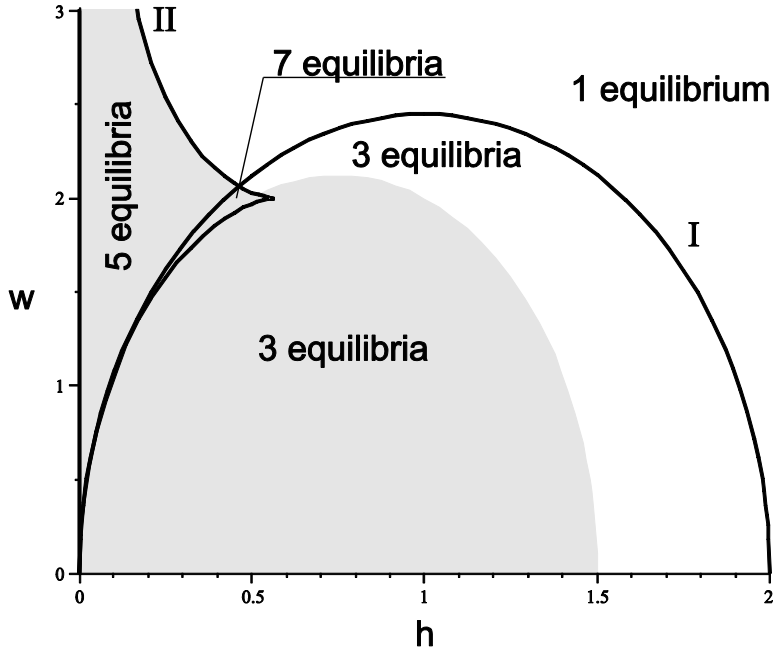


Figure 8: Total number of equilibria for the vessel. Solid lines demarcate regions with different number of equilibria. The shaded region refers to the validity domain of Case 2.

**Stability conditions**

An equilibrium position is stable or unstable if the second derivative of the potential function evaluated at the equilibrium is positive or negative, respectively (corresponding to a local minimum or maximum of the potential function)[6]. The second derivative of the potential function (10) is

$$\frac{d^2U}{d\theta^2}=\begin{cases}\left(1-\frac{h}{2}\right)\cos\theta-\frac{w^2}{24h}\left(2\cos\theta+3\sin^2\theta\cos^{-1}\theta+2\sin^4\theta\cos^{-3}\theta\right), & \text{Case 1}\\ -\frac{\sqrt{2hw}}{6}\left(\sin^{\frac{5}{2}}\theta\cos^{-\frac{3}{2}}\theta+6\sin^{\frac{1}{2}}\theta\cos^{\frac{1}{2}}\theta+\sin^{-\frac{3}{2}}\theta\cos^{\frac{5}{2}}\theta\right)+\cos\theta+\frac{w}{2}\sin\theta. & \text{Case 2}\end{cases} \quad (23)$$

The stability condition for $\theta=0$ assumes a particularly simple form:

$$\frac{d^2U}{d\theta^2}\Big|_{\theta=0} = 1 - \frac{h}{2} - \frac{w^2}{12h} > 0, \tag{24}$$

$$(h-1)^2 + \frac{w^2}{6} < 1. \tag{25}$$

The $\theta$ =0 equilibrium is therefore stable inside the elliptical region bounded by curve I in Figure 8. Even though the stability criterion (25) is local in nature, it also provides *global* information about the stability of all system equilibria. Maxima of the one-dimensional potential function cannot exist without a minimum in between, thus equilibrium solutions for the system must alternate between stable and unstable. This implies that the stability of all equilibria can be determined based on the stability of the $\theta$ =0 case alone.

To further illustrate the coexistence of equilibria for a pair of h and w and their alternating stability, Figure 9 depicts the $\theta \geq 0$ equilibria for $w$=2, $h$=0.5 and the corresponding potential function[10].

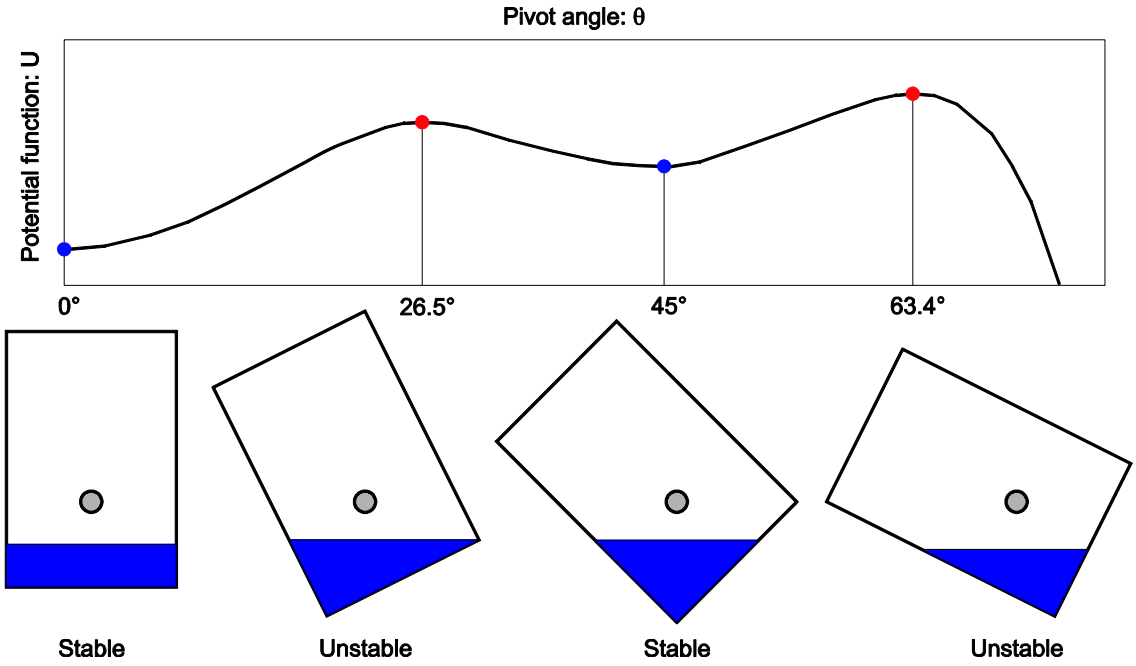


Figure 9: Coexistence of equilibria at $w$=2, $h$=0.5

# CHAPTER IV

# BIFURCATIONS AND BIFURCATION DIAGRAMS

A bifurcation, in general, refers to a qualitative change in system behavior[12]. In our context, this change is characterized by creation or destruction of equilibria. A change in the number of equilibria also corresponds to a change in the stability of a branch of equilibria. The point where the bifurcation occurs is referred to as the bifurcation point, which varies based on the parameters of the system.

To combine the information about the location and stability of equilibria, bifurcation diagrams are constructed. The bifurcation diagrams for several sets of parameters are shown in Figure 10. Note that the full diagrams are symmetric about $\theta = 0$.

There are several features on the bifurcation diagrams worth pointing out. A *pitchfork bifurcation*[5] is formed when two equilibrium branches emanate from the $\theta = 0$ equilibrium. In the previous Section we established that the $\theta = 0$ equilibrium changes from stable to unstable by crossing curve I in the h-w parameter plane (Figure 8), while two additional equilibria appear simultaneously. This pitchfork bifurcation exhibited is therefore sub-critical. Similarly, we have a sub-critical pitchfork by crossing the cusp at $w=2$, $h=9/16$ (Figure 10c).

A *saddle-node bifurcation*[7] is where a stable and unstable equilibrium points annihilate one another[12]. This type of bifurcation appears in subfigures a,b,d,e of Figure 10. The saddle-node bifurcations correspond to curve II (on which double roots of equation (16) exist) in Figure 8. The co-existence of multiple stable branches in Figure 10a-d also imply that the stable position of the vessel can become path dependent while changing the liquid level. This is the so-called *hysteresis* phenomenon.

Figure 11 shows the region around the cusp in detail. The points A through J on the *h*-*w* plane are noted on bifurcation diagrams to explicitly show their respective number of equilibria. We also label the curves where saddle-nodes (SN) and pitchforks (PF) occur.

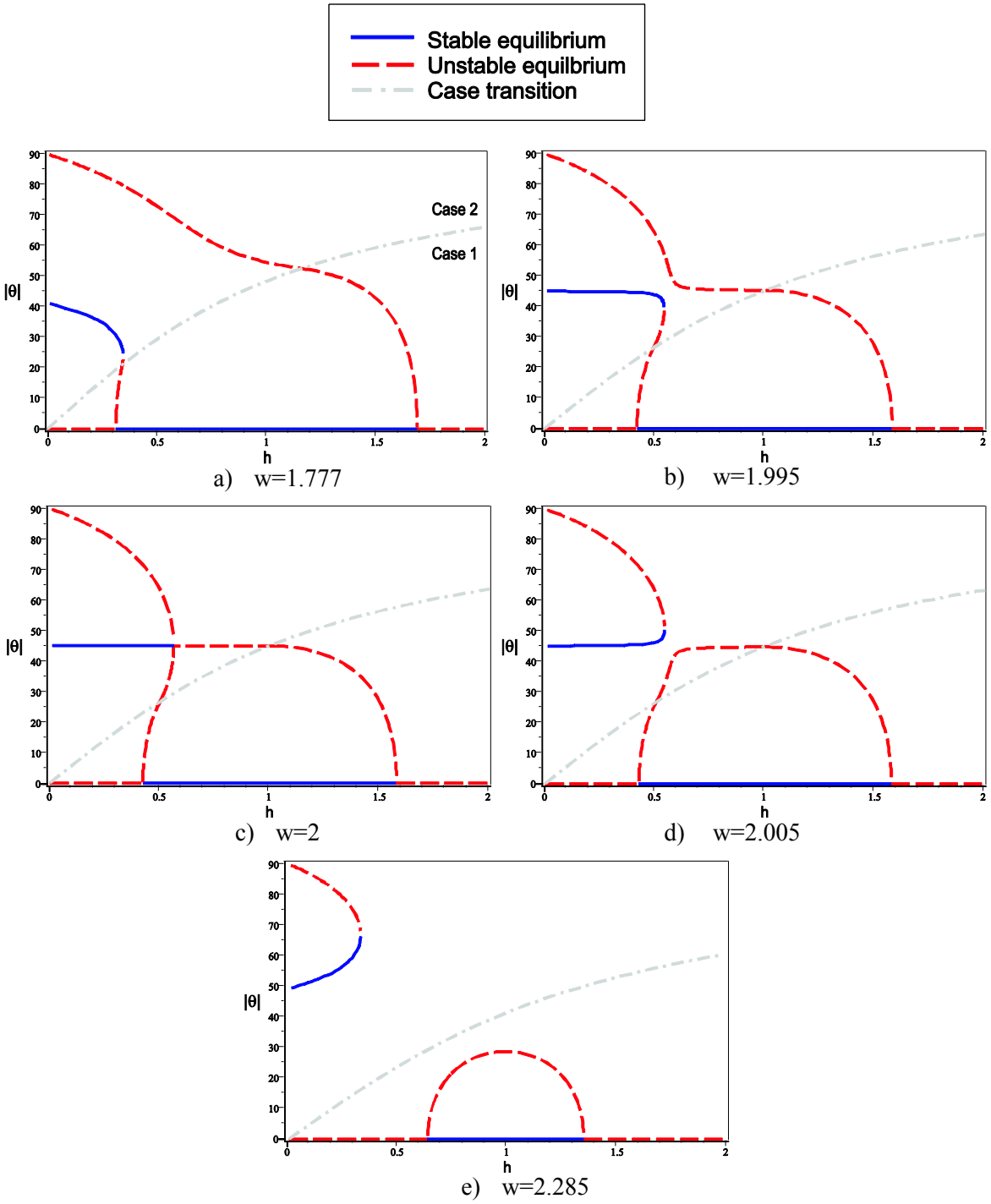


Figure 10: Bifurcation Diagrams

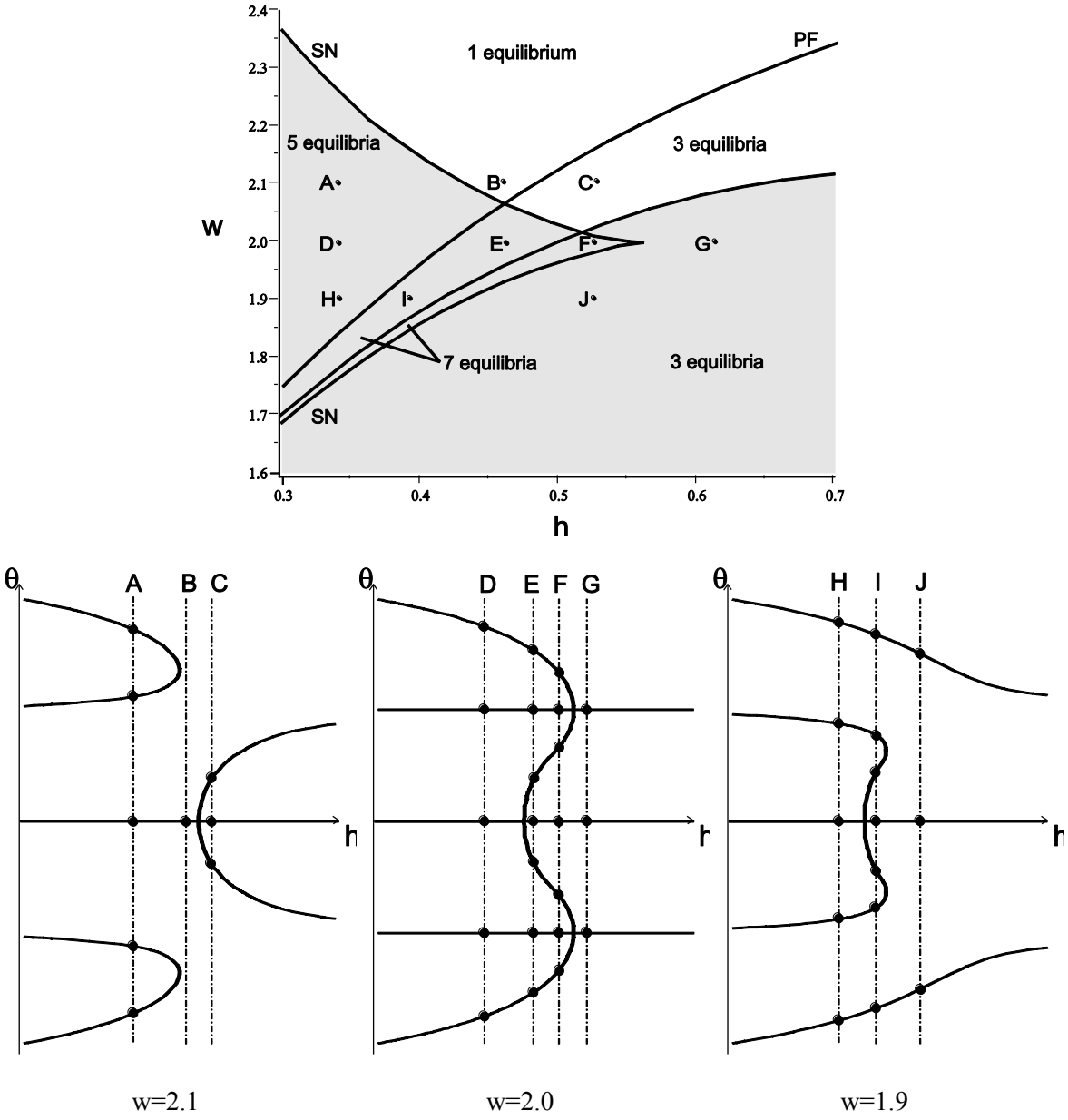


Figure 11: Unfolding of the bifurcation diagrams near the cusp. Shaded region referes to Case 2 equilibria existing.

# CHAPTER V

# EXPERIMENTAL VALIDATION

Shown in Figure 12 is the test bucket that was constructed to validate the predicted location and stability behavior of the vessel equilibrium positions. The bucket is attached to a pivot that allows rotation. The pivot can also be raised and lowered to vary the pivot height *P*.

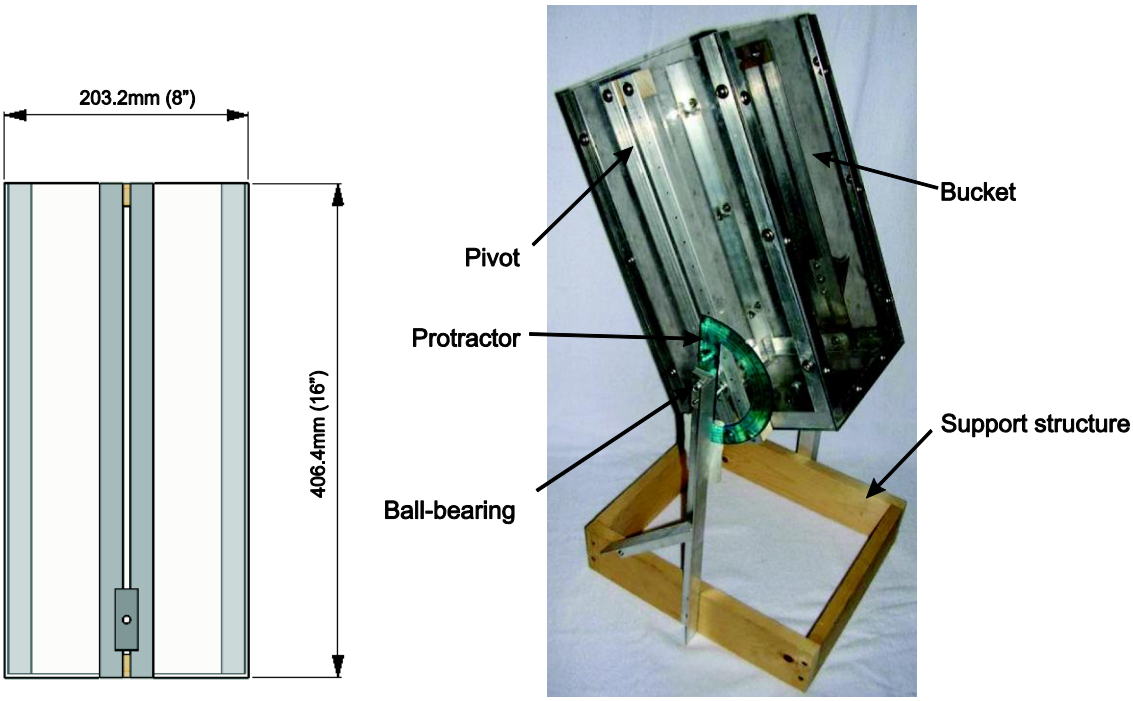


Figure 12: Test bucket design and apparatus

The bucket is constructed of Lexan sheets. The top is left open to fill and empty the bucket. For structural integrity, all of the seams are reinforced with aluminum angle bars

screwed into the corners. The seams are also sealed with silicone. On two sides of the bucket, two aluminum flat-bars form tracks for the pivot. The pivot has two clamps that grasp the tracks and can be released to adjust the pivot height. The support structure has a wooden base and two aluminum angle-bars cantilevered up to support the pivot point. At the pivot point, a ball-bearing ensures free rotation of the bucket. A good bearing is essential to get accurate and consistent results during the tests. In the theoretical derivations the wall thickness was neglected. To minimize the influence of the mass of the bucket on the measurements, the center of gravity of the bucket was adjusted to coincide with the axis of the pivot. To achieve this, steel plates were attached to the bottom of the bucket.

The first step in running the tests was to set the pivot height to a specific value. Setting this parameter accurately is crucial for the results to be accurate, because the equilibrium positions change significantly with small variations in the pivot height. The bucket was then filled with the desired amount of water. Next, the bucket was manually rotated to find the equilibrium points. The bucket settled on stable positions. Unstable positions were located by manually rotating the bucket until a point was found where the bucket tried to dump in opposite directions on either side of a point. The angles were measured by a protractor attached to the support structure.

The angles were measured with an accuracy of ±1°. The water height ($H$), pivot height ($P$), and vessel width ($W$) were measured with precision of ±1.6mm (± 1/16”), ±1.6mm (±1/16”), and ±0.8mm (±1/32”) respectively. The precision of the non-dimensional

water height ($h$) evaluates to ±0.022, and the non-dimensional vessel width ($w$) precision evaluates to ±0.032. The following diagrams are the results of three tests run on the bucket. The points shown are the test results and the lines are the calculated predictions. The uncertainty in the measurements is not shown in the results.

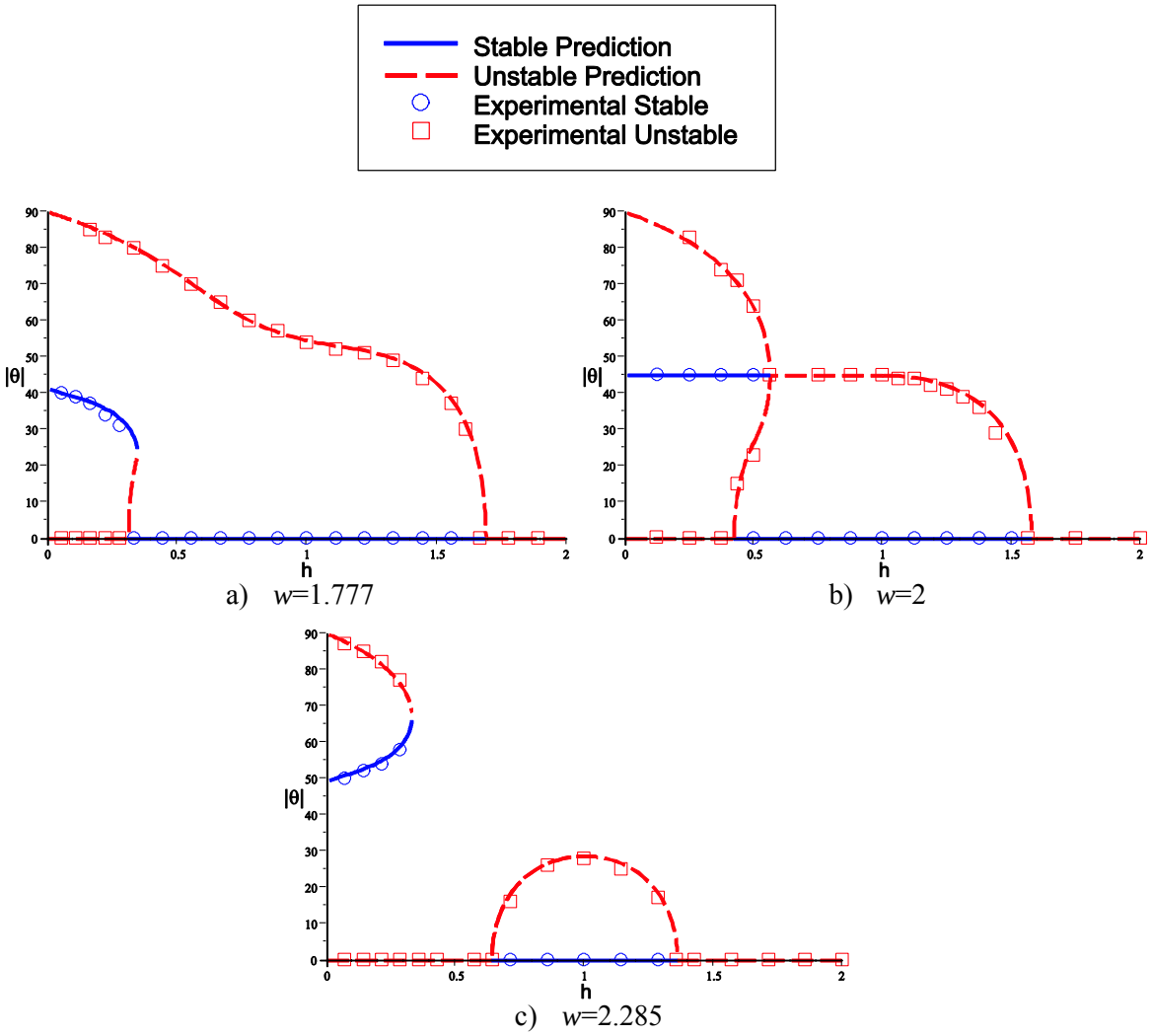


Figure 13: Experimental Results

The data from the experiments very closely follow the predicted trends. The areas which were difficult to test were where the pivot angle changes significantly with small

changes in the water height, i.e. lines with steep slopes on the diagrams. This is evident in Figure 13a where the unstable region near $h$=0.3 was not found and in Figure 13b where only two unstable states were found near $h$=0.3. It should also be noted in Figure 13c that there exists a region where no stable equilibria exist, which accounts for the bucket dumping immediately.

# CHAPTER VI

# CONCLUSION

The vessel-liquid system analyzed in this paper has been shown to have coexisting (up to seven) equilibria under many conditions. Closed-form conditions for the existence of various numbers of equilibria were given and the corresponding domains in the $h$-$w$ plane were illustrated. A simple stability condition for $\theta$=0 was also found, which also provided information about the stability of all co-existing equilibria. The existence of sub-critical pitchfork and saddle-node bifurcations were proved and bifurcation diagrams were constructed, together with a detailed unfolding of the bifurcation diagrams around the cusp point. To experimentally validate the findings, a rectangular cross-section bucket mounted on a pivot was used. Experimental data agrees very well with the theoretically predicted equilibrium positions and their stability.

# REFERENCES

[1]R. Delbourgo, "The Floating Plank," American Association of Physics Teachers **55**(9), 799-802 (September 1987).

[2]B. Duffy, "A Bifrucation Problem in Hydrostatics," American Association of Physics Teachers **61**(3), 264-269 (March 1993).

[3]P. Erdos, Paul, G. Schibler, and R. Herndon, "Floating equilibrium of symmetrical bodies and breaking of symmetry," American Association of Physics Teachers **60**(4), 335-356 (1992).

[4]E. Gilbert, "How Things Float," The American Mathematical Monthly **98**(3), 201-216 (March 1991).

[5]J. Guckenheimer and P. Holmes, *Nonlinear Oscillations, Dynamical Systems, and Bifurcations of Vector Fields,* 3rd ed., (Springer, 1990).

[6]J. Hale and H. Koçak, *Dynamics and Bifurcations,* 3rd ed., (Springer-Verlag, 1991).

[7]Y. Kuznetsov, *Elements of Applied Bifurcation Theory.* 2nd ed., Vol. 112. (Springer, 1998).

[8]H. Moseley, "On the Dynamical Stability and on the Oscillations of Floating Bodies," Philosophical Transactions of the Royal Society of London **104**, 609-643 (1994).

[9]T. Poston and J. Stewart, *Catastrophe Theory and Its Applications.* (Pitman, 1978).

[10]C. Rorres, "Completing Book II of Archimedes's On Floating Bodies," The Mathematical Intelligencer **26**(3), 32-42 (2004).

[11]G. Stepan and G. Bianchi, "Stability of Hanging Blocks," Mech. Mach. Theory **29**(6), 813-817 (1994).

[12]S. Strogatz, *Nonlinear Dynamics and Chaos,* 1st ed., (Westview Press, 2001).

[13]M. Warmowska, "Numerical Simulation of Liquid Motion in a Partly Filled Tank," Opuscula Mathematica **26**(3), 529-540 (2006).

# CONTACT INFORMATION


| | |
|---|---|
| Name: | Russell Trahan III |
| Email Address: | rtrahan3@tamu.edu |
| Education: | B.S., Aerospace Engineering<br>Texas A&M University, Dec 2010<br>Undergraduate Research Scholar |
| Address: | Department of Aerospace Engineering<br>c/o Dr. Tamás Kalmár-Nagy<br>609C H.R. Bright Building<br>Texas A&M University<br>3141 TAMU College Station, Texas 77843-3141 |